Catalysis Today 154 (2010) 75–84

Contents lists available at ScienceDirect

Catalysis Today

journal homepage: www.elsevier.com/locate/cattod

Non-equilibrium surface pattern formation during catalytic reactions with nanoscale resolution: Investigations of the electric field influence☆

J.-S. McEwen[a,*], A. Garcia Cantu Ros[a], P. Gaspard[a], T. Visart de Bocarmé[b], N. Kruse[b]

[a] Centre for Nonlinear Phenomena and Complex Systems, Campus Plaine - CP 231, Université Libre de Bruxelles, B-1050 Brussels, Belgium
[b] Chemical Physics of Materials, Campus Plaine - CP 243, Université Libre de Bruxelles, B-1050 Brussels, Belgium

ARTICLE INFO

Article history:
Available online 7 April 2010

Keywords:
Field ion microscopy
Heterogeneous catalysis
Rhodium
Platinum
Nonequilibrium oscillations
Nanopatterns

ABSTRACT

The present paper overviews our recent experimental and theoretical results concerning the catalytic properties of nanosized rhodium and platinum facets in the presence of an external electric field. We first show that field ion microcopy (FIM) experiments along with corresponding density functional theory (DFT) calculations strongly indicate that a positive field value promotes the oxidation of a rhodium field emitter tip. We also demonstrate that the catalytic oscillatory nanopatterns, as observed when H_2 and O_2 are exposed on a rhodium field emitter tip, find their origin in the different catalytic properties of all the nanofacets that are simultaneously exposed at the tip's surface. In the case of platinum field emitter tips, the dependence of dissociation barrier of NO on the external electric field is examined with DFT and compared to experimental results. Corresponding calculations on Pt are done for the $(NO)_2$ dimer.

1. Introduction

Heterogeneous catalysis by metals plays an important role in modern industrial chemistry to ensure technical progress along with sustainability. With this background it comes as a surprise that many catalytic reactions deemed to be simple have a detailed mechanism and underlying kinetics that are still unknown. While it has become clear over the years that molecules on solid metal surfaces hardly move like checkers on a checkerboard the diversity of phenomena ranging from bistability and kinetic oscillations to spatio-temporal patterns is remarkable [1–4]. To provide a sound understanding of these phenomena, surface science techniques may be employed in studies with oriented 2D single crystals [1,3,4]. However, it has been recognized that a 2D sample is morphologically an oversimplification as compared to the 3D nanosized particles usually applied in heterogeneous catalysis. Such particles are multifaceted and deposited at high dispersion on an oxide support. This difference in morphology and compositional complexity constitutes the so-called materials gap. To approximate the 3D morphology of a single nanometer-sized metal particle, in the absence of an oxide support, the apex of a field emitter tip can be considered a most suitable approach. In fact, near-atomic resolution of the tip can be achieved under the operating conditions of a field ion microscope (FIM) where an external electric field of the order of 10 V/nm is applied to either image the surface structure at low temperatures or reacting adsorbates at higher temperatures. Moreover, the field ion microscope allows studying the cooperative effects in a nonlinear chemical reaction since a large number of nanosized facets are simultaneously exposed at the surface of a 3D tip [5]. The present article is dedicated to Ben Nieuwenhuys, who has made many important contributions to understanding nonlinear catalytic surface science by using the field electron microscope [6–8].

In this paper, we will summarize our recent work that we have done by using the field ion microscope along with local chemical probing of single facets of 3D field emitter tips. We first address the catalytic formation of water from oxygen and hydrogen, which is one of the very first systems that has been studied in the framework of heterogeneous catalysis, some 150 years ago [9–11]. Despite its apparent simplicity, the underlying mechanism is still the subject of numerous investigations [12]. Recently, this reaction has received a considerable amount of attention since a surface oxide seems to form during the reaction over rhodium surfaces [13–18]. One of the underlying concerns is the correlation of the catalytic activity with the formation of this oxide layer. Interestingly, the modeling of the surface oxide in a trilayer configuration turns out to be a promising approximation susceptible to reach this goal [19,20]. On field emitter tips, a number of studies have also been reported, but an understanding of the origin of the oscillating nanopatterns has been lacking until recently [5,21]. Using the experimental and

☆ In honor of Ben Nieuwenhuys.

* Corresponding author. Tel.: +32 2 650 5798; fax: +32 2 650 5767.
E-mail address: jmcewen@ulb.ac.be (J.-S. McEwen).

0920-5861/$ – see front matter © 2010 Elsevier B.V. All rights reserved.
doi:10.1016/j.cattod.2010.02.070

theoretical tools of Sections 2 and 3, we present in Section 4 our work on rhodium field emitter tips when they are exposed to H_2 and O_2[22,23]. In particular, *ab initio* calculations on adsorbates in the presence of an external electric field will be described and a corresponding kinetic model of the bistability and the kinetic oscillations, as observed experimentally by video-field ion microscopy, will be presented. In this manner we shall demonstrate that the electric field acts at overall low pressures in a similar way as high pressures do in the absence of an electric field. While usually the formation of a surface oxide layer under UHV conditions may not be thermodynamically expected, the presence of an electric field can render it possible.

A nonlinear behavior is also observed when a platinum field emitter tip is exposed to H_2 and NO or NO_2. From the theoretical point of view, such a system with a heteronuclear molecule turns out to be even more complex as compared to the former case in which only homonuclear molecules react to form a single product molecule. In Section 5 we will present nonlinear reaction phenomena along with some new calculations involving the dissociation of NO on a stepped platinum surface. This dissociation is known to play a key role in the overall reaction mechanism and depends strongly on the local surface geometry. An interesting aspect here is the strong influence of the electric field on the reaction behavior. The interesting point for heterogeneous catalysis is that electric fields of this magnitude are comparable to those related to alkaline and earth-alkaline promoters or "simply" metal–metal oxide interfaces. Relatively low fields of several V/nm can be met in scanning tunneling microscopy (STM) measurements as well and have turned out to be sufficient to produce N_2O from NO on Pt field emitter tips at field strengths of several V/nm [24]. The N_2O formation under realistic conditions of heterogeneous catalysis is a well-known (and unwanted) phenomenon occurring on a number of different catalyst materials. More specifically, the influence of coadsorbed potassium on the NO adsorption and decomposition behavior is well documented in the literature [25].

2. Experimental setups

Two different setups were used for the experimental studies reported in this paper, which are briefly overviewed here. A detailed description of both setups can be found elsewhere [26]. In the first setup, the field ion microscope was used as a flow reactor to image, with nanometric resolution, the ongoing catalytic reactions that occur at the surface of a field emitter tip. A resolution of 2–3 Å can be obtained at cryogenic temperature conditions using an inert gas, helium or neon, as the imaging species. An example of such atomic resolution capabilities can be seen in Fig. 1. To follow the dynamics of a catalytic surface reaction, the noble gas is replaced by a flow of reactant molecules with appropriate partial pressures and a temperature sufficiently high to cause a reaction to occur. This eventually results in the observation of dynamic reaction phenomena with nanoscale lateral resolution. Rhodium or the platinum field emitter tips serving as catalyst samples are first conditioned by several cycles of field evaporation, noble gas sputtering and heat treatment before subjecting them to reaction studies. Clean tips are used as a reference to calculate the value of the field strength. The tip's radius of curvature is calculated by counting the number of atomic layers between two facets of known orientation. Standard FIM images are taken with a high dynamic range Roper Scientific CCD camera (512 × 512 pixels, 16 bits per pixel). For dynamic reaction imaging, a high sensitivity video camera with a time resolution of 20 ms is employed. Local brightnesses are then evaluated by pixel analysis of the digitized data.

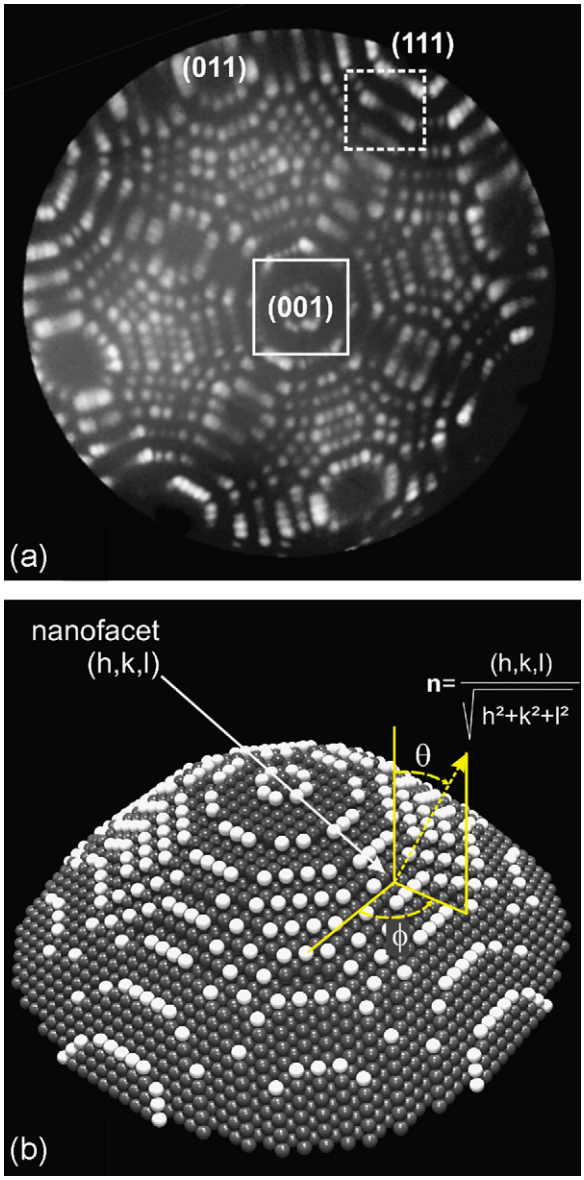

Fig. 1. (a) Field ion micrographs of a clean (0 0 1)-oriented Rh tip imaged by neon at $P_{Ne} = 10^{-3}$ Pa, $T = 55$ K, $F \sim 35$ V nm^{-1}. The radius of curvature is about 10 nm. (b) Ball model of the field emitter tip with the unit vector $\mathbf{n} = (\sin\theta\cos\phi, \sin\theta\sin\phi, \cos\theta)$ perpendicular to the nanofacet of Miller indices $(h\,k\,l)$ of an underlying fcc crystal. All the balls inside a paraboloid are retained in this model of the field emitter. We notice that the mean electric field points in the same direction $\mathbf{F} = F\mathbf{n}$ because the electric field is always perpendicular to the surface of a conductor such as the field emitter tip.

In a second setup, pulsed field desorption mass spectrometry (PFDMS) allows a chemical identification of adsorbed layers during the ongoing catalytic reaction. To do so, field pulses (~100 ns width) are applied to a counter electrode (with a hole) in front of the rhodium tip. Pulses rupture species as ions which pass the probe hole of the microscope screen and enter a time-of-flight mass spectrometer for chemical identification. Pulse amplitudes may vary and can be adjusted such that the dynamics of a catalytic reaction are visibly not influenced. On the other hand, field pulse amplitudes may be high so as to ensure quantitative field desorption and to determine surface coverages. A "reaction field" can be maintained between pulses. Varying this field provides insight into the field dependence of adsorption and reaction processes.

3. Theory

3.1. O_2–H_2 reaction on Rh

A kinetic mean field model has been developed to model the observed non-linear phenomena when a rhodium field emitter tip is exposed to O_2 and H_2. Details are presented elsewhere [22,23]. Here we limit ourselves with an outline of the reaction scheme:

adsorption and desorption of hydrogen:

$$H_2(\text{gas}) + 2\varnothing(\text{ad}) \underset{k_{dH}}{\overset{k_{aH}}{\rightleftharpoons}} 2H(\text{ad}) \tag{1}$$

diffusion of hydrogen:

$$H(\text{ad}) + \varnothing(\text{ad}) \overset{k_{diff}}{\rightleftharpoons} \varnothing(\text{ad}) + H(\text{ad}) \tag{2}$$

adsorption and desorption of oxygen:

$$O_2(\text{gas}) + \text{surface} \underset{\tilde{k}_d}{\overset{\tilde{k}_a}{\rightleftharpoons}} O_2(\text{pre}) + \text{surface} \tag{3}$$

dissociation and recombination of oxygen:

$$O_2(\text{pre}) + 2\varnothing(\text{ad}) \underset{k_d}{\overset{k_a}{\rightleftharpoons}} 2O(\text{ad}) \tag{4}$$

oxidation and reduction of rhodium:

$$O(\text{ad}) + \varnothing(\text{sub}) \underset{k_{red}}{\overset{k_{ox}}{\rightleftharpoons}} \varnothing(\text{ad}) + O(\text{sub}) \tag{5}$$

reaction of water formation:

$$2H(\text{ad}) + O(\text{ad}) \overset{k_r}{\rightarrow} 3\varnothing(\text{ad}) + H_2O(\text{gas}) \tag{6}$$

The adsorption of hydrogen on rhodium is dissociative and its desorption associative in Eq. (1). The relative rates of associative desorption (k_{dH}), dissociative adsorption (k_{aH}) and diffusion of hydrogen (k_{diff}) on the various nanofacets of the tip will determine how fast these processes evolve during the reaction. Hydrogen diffusion on rhodium under our experimental conditions, see Eq. (2), turns out to be a very fast process.

For oxygen, we take into account its dissociative adsorption ($\tilde{k}_a$) and associative desorption ($\tilde{k}_d$) into an intrinsic or an extrinsic precursor state in Eq. (3). Once in the precursor state, oxygen can dissociate and chemisorb onto the surface (k_a), as described by Eq. (4). Correspondingly, an adsorbed oxygen atom can combine with another adsorbed oxygen atom into the precursor state (with the corresponding rate k_d).

Moreover, to describe the formation of a surface oxide trilayer O(ad)–Rh–O(sub), the adsorbed oxygen atoms are supposed to penetrate the surface if they become sufficiently abundant in the adlayer. In this respect, the formation of the oxide trilayer corresponds to the oxidation and reduction of rhodium with the respective rates k_{ox} and k_{red} in Eq. (5).

Finally, exposing the rhodium crystal to both oxygen and hydrogen allows the catalytic formation of water on rhodium. For this reaction, experiments on platinum [12] and on rhodium [27,28] have demonstrated that we can here neglect the OH intermediate and consider the simplified reaction given by Eq. (6).

In our previous work [22,23], we have shown that the rate coefficients and their activation energies on several of the main crystal planes are structure dependent. As a consequence, the anisotropy of the field emitter tip will necessarily imply that the rates of the chemical processes occurring on its surface will be anisotropic as well. In our mean field model, this structure dependence is taken into account by determining, for each catalytic reaction, how the activation energy E and the prefactor k^0 of each rate coefficient depend on the unit vector $\mathbf{n}$ perpendicular to the crystalline plane:

$$k = k^0(\mathbf{n}; F) \exp\left[-\frac{E(\mathbf{n}; F)}{k_B T}\right] \tag{7}$$

where F is the electric field at the surface, T is the temperature, and k_B Boltzmann's constant. The normal unit vector $\mathbf{n}$ itself depends on the Miller indices $(h\,k\,l)$ of the nanofacet where the reaction takes place (see Fig. 1). Since the Miller indices vary for the different nanofacets composing the field emitter tip's surface, the rate coefficients, as given in Eq. (7), have the desired spatial dependence describing the anisotropy of the crystalline tip. Regarding the values of the kinetic parameters, they are fixed so as to be in line with *ab initio* calculations and experimental data. In particular, we obtain these values by investigating the low Miller indexed surfaces, namely Rh{0 0 1}, Rh{0 1 1} and Rh{1 1 1} [23]. The corresponding values for the remaining nanofacets can be interpolated by expanding each relevant prefactor or activation energy into the so-called kubic harmonics [29] for the underlying fcc crystal.

We note that in Eq. (7), the normal unit vector $\mathbf{n}$ and the electric field F are defined with respect to the *mean* shape of the tip (here taken as a paraboloid). Such an approach is justified since the atomic scale (Rh and Pt lattice constants of 0.38 and 0.39 nm, respectively) is significantly smaller than the scale of the nanopatterns and the tip's radius of curvature (~10 nm).

To gain an atomistic understanding of the underlying reaction mechanisms, density functional theory (DFT) calculations were performed with the Vienna *ab initio* simulation package (VASP), a plane-wave DFT program which is based on the projector augmented wave method [30–32]. The computational details for the calculations involving oxygen interaction with rhodium are given in Ref. [33].

3.2. NO–H_2 reaction on Pt

This reaction was investigated by FIM as one of the firsts in our laboratory. A mean-field approach based on a reaction model involving NO and H_2 dissociative adsorption followed by N_2 and H_2O associative desorption was mounted subsequently [34]. The surface reactions leading to these molecules were lumped together

$$2H(\text{ad}) + NO(\text{ad}) \rightarrow 4\varnothing(\text{ad}) + \tfrac{1}{2}N_2(\text{ad}) + H_2O(\text{gas}) \tag{8}$$

to demonstrate that the autocatalytic behavior is related to the liberation of empty sites. The model allowed understanding the occurrence of multiple reaction states and explosive ignition phenomena in the formation of water on a Pt{0 1 2} facet without consideration of surface diffusion. Furthermore, the influence of the external electric field has not been considered in Ref. [34], despite the experimental observation of nitrous oxide (N_2O) and nitrogen formation during the interaction of NO with the (1 1 1) pole of a Pt field emitter tip [24]. Thus, a detailed understanding of the non-linear reaction mechanism on platinum field emitter tips is still missing to a large extent. To fill the gap in knowledge of the detailed mechanism, we have recently started to study the interaction of NO with stepped Pt surfaces using DFT. Some of the results will be presented here to demonstrate the need for the inclusion of electric field effects in mounting a realistic reaction model.

We have selected Pt{2 2 3} and Pt{0 1 1} (1 × 2) to study NO adsorption. To do so, a cut-off energy for the expansion of the plane waves 400 eV was found sufficient for an accurate calculation of the binding energy. For NO dimerisation to $(NO)_2$ on Pt{2 2 3} a slightly lower energy cut-off of 340 eV was used. The climbing image nudged elastic band method was applied when calculating the activation energies [35]. This helped to determine the activation energies that enter into the kinetic model and their resulting dependence on the external electric field.

4. Catalytic formation of water on rhodium

4.1. Field-assisted oxidation on rhodium

In our previous work [33], we followed the oxidation of nano-sized rhodium facets in the presence of a high external electrical field using a FIM. Corresponding density functional theory calculations were done using the O–Rh–O surface oxide trilayer approximation on a Rh{0 0 1}, Rh{0 1 1} and Rh{1 1 1} surface. Introducing effective dipole values into a kinetic model the self-sustained oscillations as observed while oxygen and hydrogen were reacting to form water, could be successfully described [22,23]. Before briefly overviewing this work, we will consider two natural extensions of such results:

(i) the nonlinear induced charge changes of the electron charge density
(ii) the influence of a negative electric field on the activation barriers

These questions will be addressed by considering the stepwise reduction of the number of oxygen atoms in the c(2 × 8) trilayer O–Rh–O surface oxide on Rh{0 0 1} [14]. This corresponds to the experimental observation that surface oxide layers in heterogeneous catalysis are non-stoichiometric rather than stoichiometrically well behaved. With this background, we calculate the energy difference between a situation with two nearest neighbor vacancies in the inner layer [denoted henceforth as the trilayer–($2O_s$)] with respect to a situation where both the outer and the inner oxygen layers have a vacancy at nearest neighbor distances from each other [i.e., a trilayer–(O_s+O) structure, which is partly depicted in Fig. 2], as we did in our previous work [33]. We also calculate the energy barrier between these two states and focus our attention on the Rh{0 0 1} surface, since our previous investigations show that the energy barriers between these two states have a strong dependence on the external electric field.

We first address the nonlinear induced changes of the electron charge density. Such a nonlinear change will be reflected in the corresponding activation energies. In our previous work [33], we have limited ourselves to a moderate field of 4 V/nm to obtain convergence in calculations. Here we increase the electric field slightly from 4 V/nm to 6 V/nm when examining the induced nonlinear charge changes without running into convergence problems. Note, however, that the external electric fields while imaging the oxygen–hydrogen reaction are at least 9–10 V/nm.

The reaction path can be defined by the movement of an oxygen atom. In the calculations of the energy barriers, we additionally fix the z position of the oxygen atom for the various intermediate configurations. We depict in Fig. 2 the electric field dependence of the hopping barrier for an oxygen atom to go from the outer oxygen layer to the transition state ($E_{in}^{\ddagger}$) which is decreased in the presence of external electric field. Similarly, the hopping barrier to go from the inner oxygen layer to the transition state ($E_{out}^{\ddagger}$) decreases as well in the presence of an external electric field, but not as significantly. As for the z position of the transition state, it is situated near the rhodium layer position within the oxide in the absence of an external electric field while it occurs at a smaller z value when a positive electric is applied. As can be seen from Fig. 2, the dependence of $E_{in}^{\ddagger}$ and $E_{out}^{\ddagger}$ on the external electric field is nonlinear. Indeed, by extrapolating the situation between F = 0 V/nm and 4 V/nm, as in our previous work, we would infer barriers at 6 V/nm of 2.328 eV and 1.787 eV for $E_{in}^{\ddagger}$ and $E_{out}^{\ddagger}$, respectively. However, Table 1 shows that the barriers at 6 V/nm are significantly lower at 2.119 eV and 1.567 eV. Thus, the dependence is clearly nonlinear. As a consequence, one might expect an even more drastic decrease of the energy barriers at the experimental values of 9–10 V/nm as com-

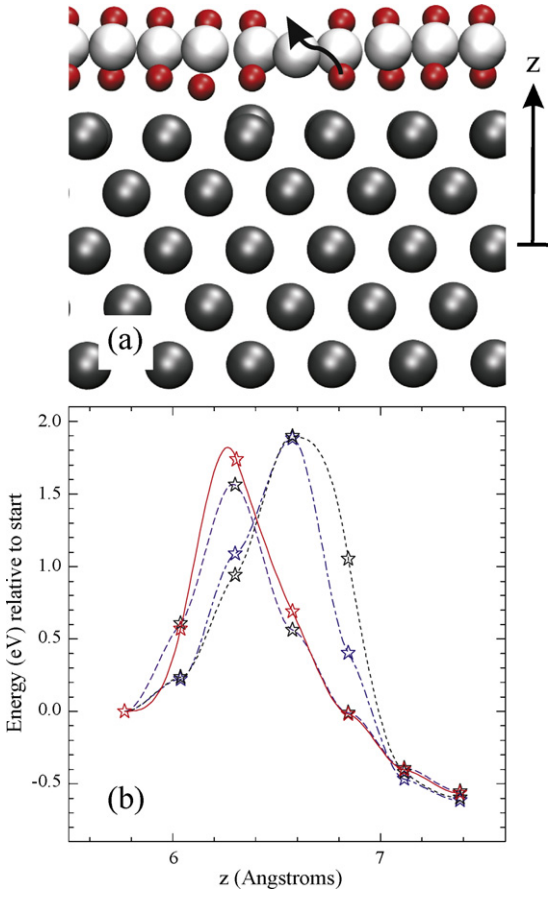

Fig. 2. (a) The initial configuration on Rh{0 0 1} in the DFT calculations. The arrow beginning from an oxygen atom indicates the reaction pathway starting from the inner oxygen layer to the outer one. The value of z is relative to the position of the closest fixed rhodium layer of the underlying substrate. The grey spheres are rhodium atoms, the white spheres are rhodium atoms in the oxide layer, while the small grey spheres (red online) are oxygen atoms. (b) The hopping barrier for an oxygen atom to go from the inner to the outer oxygen layer (increasing z) within a surface trilayer oxide with two oxygen vacancies on an underlying Rh{0 0 1} surface using the generalized gradient approximation (GGA) according to Perdew et al. [75]. The surface was modeled with slabs consisting of five rhodium layers with the bottom three layers fixed at the theoretical bulk lattice constant of a = 3.844 Å. The vacuum thickness was at least ~11 Å. The lines are cubic spline interpolations between the intermediate values at an electric field of 6 V/nm (dashed line), 4 V/nm (solid line), 0 V/nm (dotted line) and −4 V/nm (dash-dotted lines) [22,23]. (For interpretation of the references to color in this figure legend, the reader is referred to the web version of the article.)

Table 1
The activation energies (eV) versus the applied electric field (V/nm) for the passage of an oxygen atom from an adsorbed state to one that is subsurface in the presence of a surface oxide trilayer. The calculations are performed using the nudged elastic band method [35].

Surface	Rh{0 0 1}
$E_{in}^{\ddagger}$ ($F = -4$ V/nm)	2.494
$E_{out}^{\ddagger}$ ($F = -4$ V/nm)	1.880
$E_{in}^{\ddagger}$ ($F = 0$ V/nm)	2.490
$E_{out}^{\ddagger}$ ($F = 0$ V/nm)	1.895
$E_{in}^{\ddagger}$ ($F = 4$ V/nm)	2.383
$E_{out}^{\ddagger}$ ($F = 4$ V/nm)	1.820
$E_{in}^{\ddagger}$ ($F = 6$ V/nm)	2.119
$E_{out}^{\ddagger}$ ($F = 6$ V/nm)	1.567

pared to those extrapolated by comparing the results at 0 V/nm and 4 V/nm.

We now look at the influence of a negative electric field on the oxidation barrier on a Rh{0 0 1} surface. Such an investigation is of interest since an oscillating reaction behavior along with nanopatterns formation have also been observed on rhodium when it is exposed to NO and H_2 under field electron microscopy (FEM) conditions [6–8]. The underlying mechanism of this oscillatory behavior has also been investigated in a corresponding mathematical model [36]. We depict in Fig. 2 the influence of the barrier when a negative electric field of −4 V/nm is applied. We note that this field strength is higher to what is applied in an FEM. As for the barrier, it does not decrease remarkably when we invert its polarity, in contrast with the positive electric field situation. Thus, the presence of subsurface oxygen, as observed in the corresponding photoemission electron microscopy experiments [37], seems not to be influenced significantly by the presence of a negative external electric field.

4.2. Bistability and oscillating nanopatterns

As is well known, autocatalytic processes can exhibit a wide variety of complex behaviors, ranging from the emergence of multiple stationary solutions, to oscillations and chaos in both time and space. The origin of such phenomena lies in the structural instabilities that occurs in the dynamics of the system [38]. Such complex behaviors emerge in a number of systems in nature. As under Section 4.1 we inspect here the oxygen–hydrogen reaction on Rh as a simple yet important system of heterogeneous catalysis. We have previously modeled this system successfully to understand the nanoscale pattern formation that it provokes [39,40].

One of the scenarios for the observation of an oscillatory behavior is the occurrence of nearby hysteresis effects in the catalytic water production [41]. Such effects are manifest in the different P_{H_2}/P_{O_2} pressure ratios necessary to establish the same water production while increasing or decreasing these ratios. According to the experimental observations, small P_{H_2}/P_{O_2} pressure ratios favor the (dissociative) adsorption of oxygen along with surface oxidation, whereas large P_{H_2}/P_{O_2} ratios lead to (dissociative) hydrogen adsorption. In an intermediate region, the system becomes bistable and a hysteresis behavior extends over a certain P_{H_2}/P_{O_2} range, which narrows with increasing temperature. This defines the bistability region, which is depicted in Fig. 3 in between 400 K and 550 K. At 550 K, when the bistability diagram has considerably narrowed and P_{H_2}/P_{O_2} is of the order of unity, the emergence of self-sustained oscillations can be observed [39,40]. The nanopattern formation associated with the oscillatory water production turns out to be related with the reversible surface oxidation of the Rh nanoparticle. Direct proof of the change in surface composition has been provided by atom-probe mass spectrometry. Accordingly, once the surface undergoes oxidation, RhO_x ($x = 1, 2$) species can be field desorbed as ions during the undergoing reaction (and without visibly disturbing it). In this way, a direct correlation of the local catalytic water production with the brightness of the field ion micrographs become possible [39,40]. A reliable correlation must, however, take into consideration the influence of the electric field which is a variable of state like pressure or temperature. According to our recent work, the bistability region indeed enlarges once the electric field is switched on, see Fig. 3. Thus the facet-dependent rate coefficients as given by Eq. (7) vary nonlinearly and using an Arrhenius ansatz this translates into a field dependence of the activation energy barriers.

As to the oscillations, which occur once the reaction conditions approach the bistability cusp in Fig. 3, more recent experiments have shown that the oxygen ionization may contribute significantly to the image once the reaction cycle runs into the catalytically less active state of a surface oxide. In fact, this leads us to compare the field ion micrographs with the corresponding subsurface

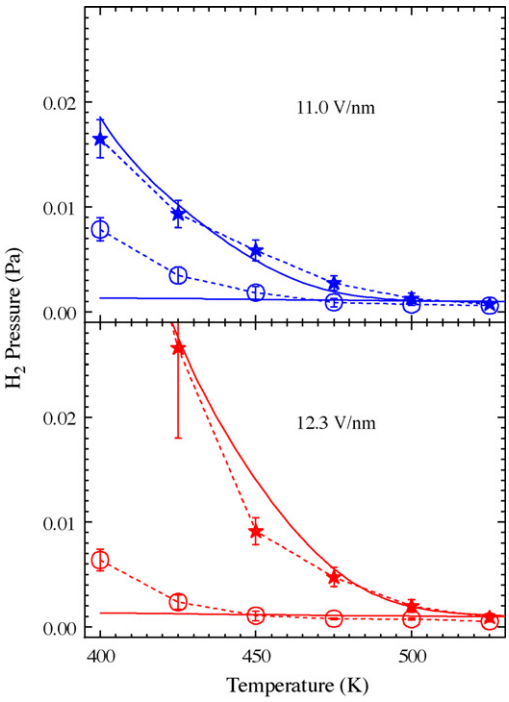

Fig. 3. (a) The bistability diagram showing hysteresis for $P_{O_2} = 5 \times 10^{-4}$ Pa during catalytic water formation on rhodium at 11.0 V/nm and (b) 12.3 V/nm. The circles and stars indicate the experimental pressures (with corresponding error bars) for which the structural transformation occurred when decreasing and increasing the hydrogen pressure, respectively. The area in between marks the coexistence region of bistability. The full lines mark the theoretical delimitation of the bistability region with a kinetic model of the field emitter tip.

oxygen distribution as obtained within our model. The situation is depicted in Fig. 4, in which a stunning agreement between theory and experiment is obtained.

4.3. Catalytic activity: metal, surface oxide and bulk oxide

The correlation of the catalytic activity of the metal with the presence or the absence of the surface oxide has been examined in several studies with single crystal rhodium surfaces [42–45]. A number of such studies have also correlated the active phase with the presence of the surface oxide [44,46]. On the other hand, the bulk Rh_2O_3 oxide is found to be catalytically inactive [45]. Moreover, in a recent report, it has been suggested that the catalytic activity of the O(ad)–Rh–O(sub) oxide with H_2 is similar to the reactivity of the surface oxide with CO [20]. On a rhodium field emitter tip a surface oxide seems to be formed as well. This is indicated by the detection of RhO_x species in the atom-probe and the occurrence of RhO_2 precipitates in high resolution transmission electron microscopy experiments [47]. Thus, an O(ad)–Rh–O(sub) surface oxide would seem to be a reasonable approximation for a Rh field emitter tip and we would expect that such a phase would be catalytically more active than the metallic phase. However, this turns out not to be the case since according to the field ion microscopic observations the metallic phase is more active than the oxide phase [39,40]. The apparent incompatibility of the results is removed when considering that the FIM experiments are done under reaction conditions with temperatures between 520 and 550 K while those reported for low Miller indexed surfaces [20] refer to room temperature. Thus the amount of surface hydrogen in the latter studies was much more significant than in the FIM studies. To recall, hydrogen desorbs at around 300 K on Rh{0 0 1} [48]. Given the relatively small plane-to-plane variation of the hydrogen adsorption energy, its coverage on a metallic rhodium field emitter tip can be

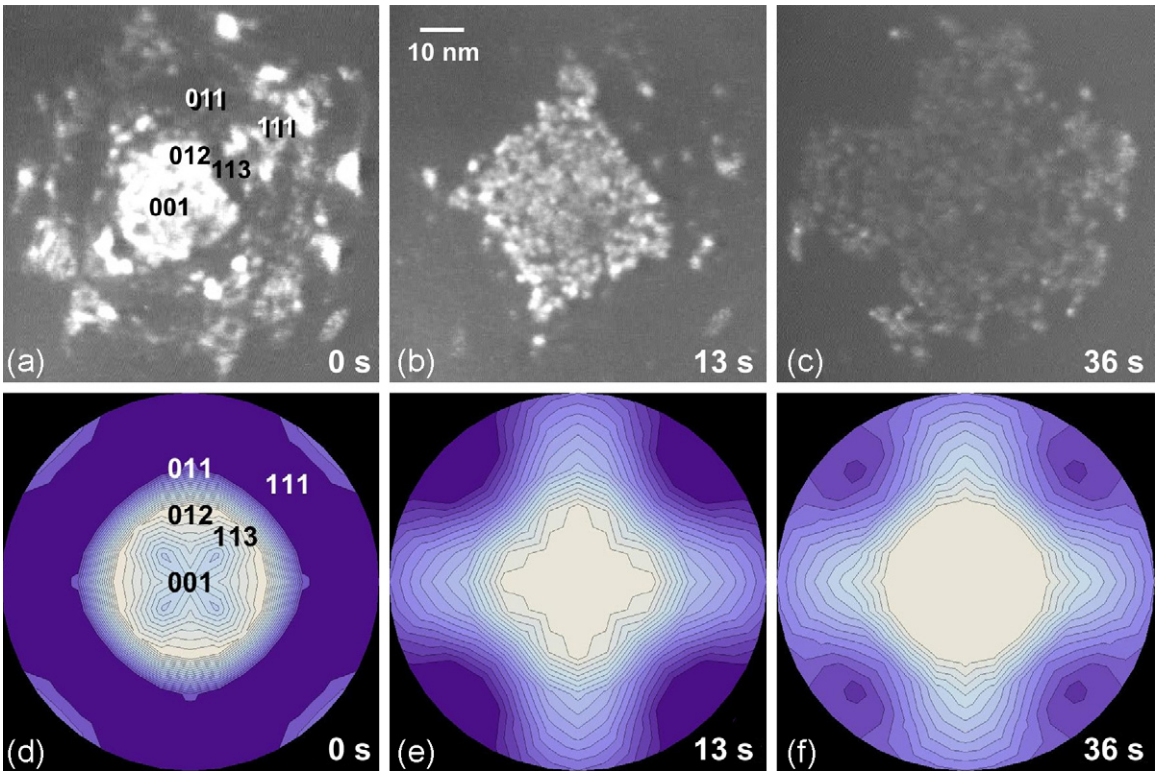

Fig. 4. Series of FIM micrographs covering the complete oscillatory cycle as well as the corresponding time evolution of the subsurface oxygen distribution on a logarithmic scale as obtained within a kinetic model of the reaction over the field emitter tip. Starting from a surface in the quasi-metallic state (a) and (d), an oxide layer invades the topmost plane and grows along the {0 1 1} facets forming a nanometric cross-like structure (b) and (e). The oxide front spreads to finally the whole visible surface area (c) and (f). The temperature, electric field and partial pressures of oxygen in panels are $T = 550$ K, $F_0 = 12$ V/nm, $P_{O_2} = 2 \times 10^{-3}$ Pa, respectively. On the other hand, the hydrogen pressure is $P_{H_2} = 2 \times 10^{-3}$ Pa in the FIM experiments and 4×10^{-3} Pa in our kinetic model. For the subsurface site occupation, the white areas indicate a high site occupation value while the dark areas indicate a low site occupation value [22,23].

estimated to be around 0.01 ML at 550 K. When the oxide is formed on the tip, the hydrogen coverage will be significantly smaller compared to the metallic phase. In the former case, the corresponding turnover frequency for water formation will be high while in the latter it will be low so that the apparent discrepancy between our results and those obtained by Gustafson et al. [44] indeed disappears. Moreover, as mentioned above, the low catalytic activity of the oxide phase, as observed on a rhodium field emitter tip, resides in the possibility that further oxidation and RhO_2 local precipitation take place during the oscillations. The model of a O(ad)–Rh–O(ad) surface oxide would appear as a rough approximation and should probably be replaced by a double trilayer structure such as the ORhO–4L structure for Rh{1 1 1}, which is largely inactive. Experimentally, we consider the 3D atom probe (3DAP) to be ideally suited to perform a layer-by-layer composition analysis [49]. Indeed, such a probe can provide both chemical and atomic-scale positional mapping of field emitter tips [49].

In conclusion, much has been recently learned and understood about the oscillatory hydrogen–oxygen reaction on Rh 3D nanosized samples. The inclusion of field effects in the theoretical modeling along with the approximation of a O(ad)–Rh–O(sub) configuration for a surface oxide turned out to be key to the success. Particularly interesting from the viewpoint of heterogenous catalysis seems to be the fact that the electric field promotes surface oxidation of Rh under overall UHV or HV conditions. As the upper limit of gas pressures in the FIM is of the order of 10^{-3}mbar this field effect might be used to produce surface and near-surface chemical compositions that otherwise are only achievable in high-pressure studies. This idea will provide the incentive for further FIM studies in the future, coupled to rigorous theoretical modeling.

5. Field effects in the dissociation of NO on Pt

The incentive to investigate the field influence on NO adsorption is provided by the observation of multiple reaction states along with erratic fluctuations during the reaction of NO with hydrogen on a Pt field emitter tip [50]. A nonlinear behavior also occurs in the absence of fields using Pt low Miller index single crystals. On a flat Pt{0 0 1} surface, regular self-sustained oscillations have been observed by several groups and mathematical models put forward to explain the observed behavior [51–53]. On a (0 0 1) oriented platinum 3D nanosized tip, spatial–temporal patterns are observed with corresponding surface explosions around the {0 1 2} planes [50]. An example of such a surface explosion is shown in Fig. 5. The chemical reaction underlying this explosion is described by Eq. (8). The production of a larger amount of empty sites than actually needed per reaction cycle causes the adsorbed layer to react off fast. NO molecules adsorbed in neighboring areas rush into empty sites and cause an increase of the image brightness due to their efficient field ionization [50]. Eventually, a fast-moving reaction from {0 1 2} toward the central (0 0 1) pole can be observed (see Fig. 5) before a catalytically less active state is entered. However, as can also be seen in Fig. 5, these explosions do not occur regularly in time. In fact, they can be shown to occur randomly according to a Poissonian distribution [54]. A mean field model by De Decker et al. has been put forward to explain the occurrence of such phenomena, but as mentioned in Section 3.2, the presence of the external field was not taken into account [34] despite their obvious importance in provoking the explosive phenomena [50].

Interestingly, in the absence of H_2, the presence of the external electric field has been revealed to fundamentally alter the underlying chemical processes taking place on the Pt surface. While in

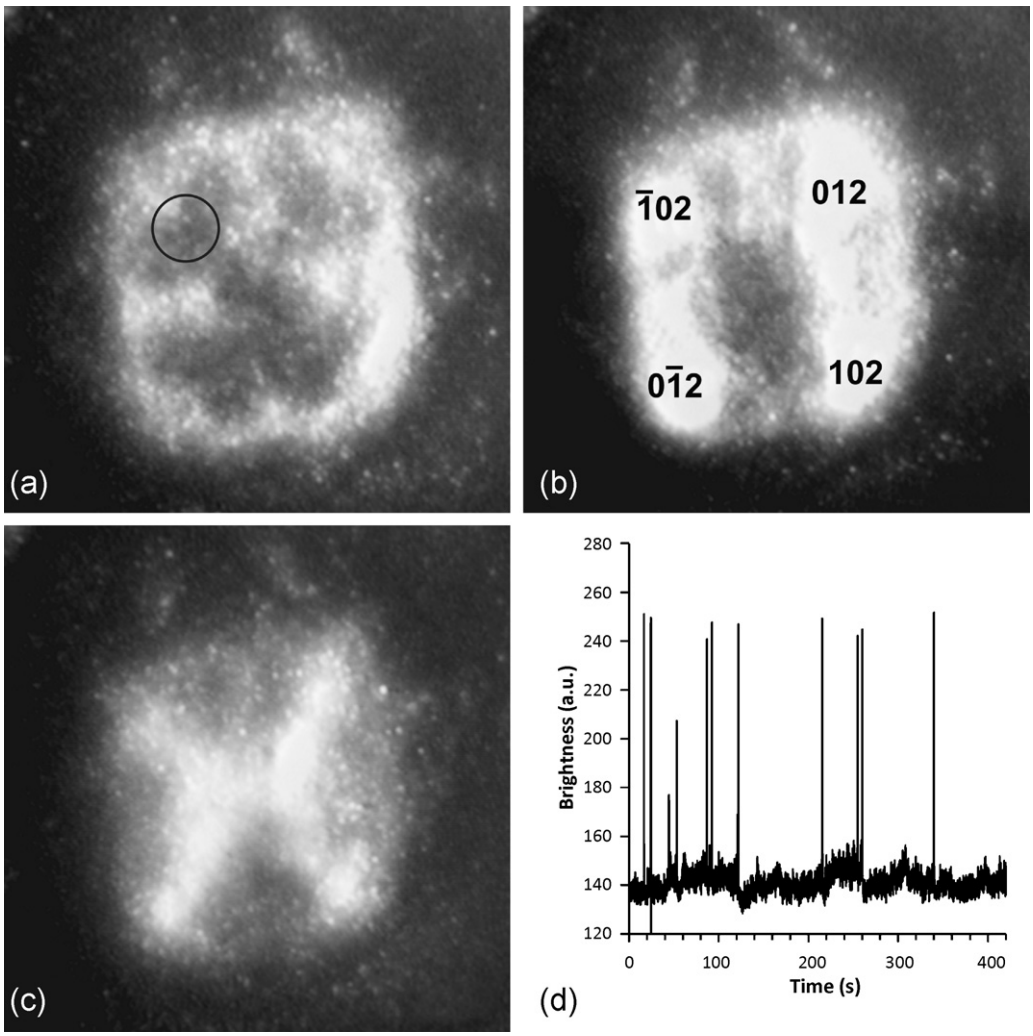

Fig. 5. Sequence of FIM micrographs illustrating the occurrence of explosive phenomena, experimental conditions: $T = 525$ K, $P_{H_2} = 4 \times 10^{-3}$ Pa, $P_{NO} = 2.5 \times 10^{-3}$ Pa, $F \sim 9$ V/nm [50]. (a) The surface before the explosion followed by (b) a concerted ignition of the {0 1 2} planes. This front then moves to the (0 0 1) pole in panel (c). The time elapsed between the three sequences is less than 1.2 s. (d) The time evolution of the brightness when probing the area indicated in panel (a) where each spike represents one explosive reaction.

the absence of a steady electric field (F_R) atom probe experiments with NO on a (stepped) {1 1 1} plane of a Pt field emitter tip at 296 K only yield molecular NO^+, species like N_2O^+ and N_2^+ occur in the presence of F_R (see Fig. 6). Thus, NO adsorbs in its molecular form in the absence of F_R, whereas association and dissociation processes occur in its presence [24]. A theoretical analysis of this behavior has also been performed by Kreuzer and Wang [55].

A number of *ab initio* calculations involving the dissociation of NO on Pt surfaces exist in the literature, such as on Pt{1 1 1} [56,57] and Pt{0 0 1} [58,59] as well as on stepped surfaces [56,60,62]. It is generally agreed upon that Pt{1 1 1} and Pt{0 1 1} (1×2) are essentially inert toward the dissociation of NO, while Pt{0 0 1} is more active [62]. On vicinal surfaces, such as Pt{1 1 2} or Pt{0 1 4}, the dissociation of NO is also found to occur [56,62]. Moreover, it has been suggested in the literature that NO dissociates more easily on stepped surfaces composed of {0 0 1} steps and {1 1 1} terrace sites [60].

For our calculations, we have chosen to examine the dissociation of the NO molecule on a Pt{2 2 3} surface, which consists of five rows of terrace atoms of {1 1 1} geometry and then a row of step atoms of {0 0 1} geometry. On a field emitter tip, the Pt{2 2 3} facet is close to the {1 1 1} within the zone line joining the {0 0 1} plane with the {1 1 1} plane, see Fig. 1. This area is representative for the probe hole experiments described above. As shown in Fig. 7, we also

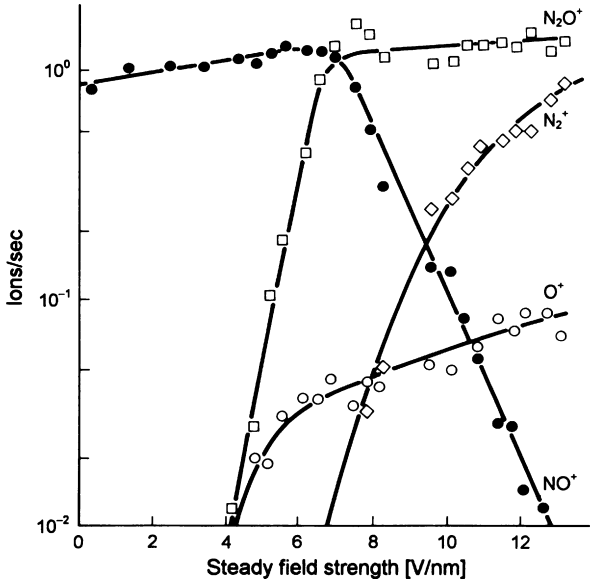

Fig. 6. Field-induced decomposition of NO on Pt, measured on a stepped surface with {1 1 1} orientation terraces. $P_{NO} = 6.7 \times 10^{-5}$ Pa, $T = 296$ K [24].

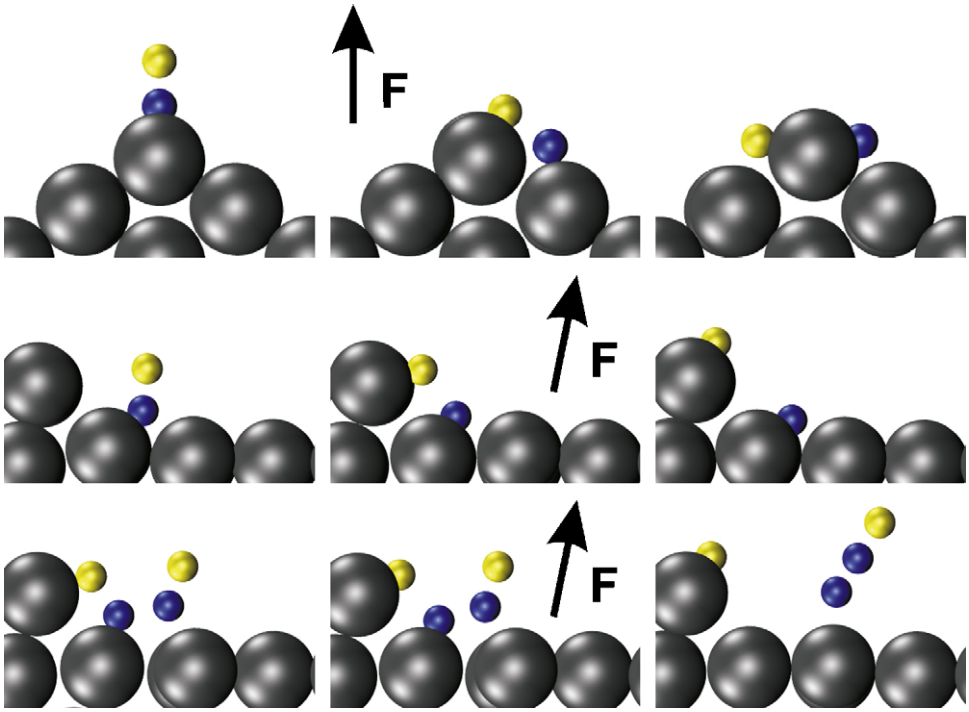

Fig. 7. Possible dissociation pathways for NO on Pt{0 1 1} (1 × 2) (top), NO on Pt{2 2 3} (middle) and $(NO)_2$ on Pt{2 2 3} (bottom). The images on the left, middle and right represent respectively the molecularly adsorbed state, the transition state and the dissociated product. The positions of the atoms as shown in the figure are optimized in the absence of a field. The large grey spheres are the Pt atoms, the small light grey spheres (yellow online) are the O atoms while the small dark grey spheres (blue online) are the N atoms. The direction of the applied external electric field is normal the surface, so that on the {2 2 3} plane it is at an angle of 11.42° with respect to the {1 1 1} plane, as depicted in the Figure. (For interpretation of the references to color in this figure legend, the reader is referred to the web version of the article.)

consider the process involving the dissociation of NO at the base of the step along with the corresponding final state. Although we find that it is energetically less favorable by 0.785 eV to have NO at the base of the step than at the step edge, the overall barrier of this dissociation mechanism has been found to be the lowest among the other possible reaction pathways on Pt{1 1 2} [62] and Pt{3 3 5} [60] (which only differ from the Pt{2 2 3} surface by their respective terrace widths). Moreover, such a configuration is similar to the one envisaged by Kreuzer and Wang [55] and brings the O atom closer to the metal surface.

In the absence of an externally applied electric field, dissociation at the base of the step is more favorable than molecular NO adsorption, as it was found to be the case on Pt{1 1 2} [62] and Pt{3 3 5} [60]. However, this energy difference decreases when the field is switched on: While in the absence of a field the energy difference between the initial and the final state is 0.166 eV in favor of the dissociated product this energy difference decreases to 0.123 eV at $F = 5$ V/nm and 0.096 eV at $F = 8$ V/nm. It is also instructive to compare these results with those for other surfaces. On a Pt{0 1 1} (1 × 2) surface, NO binds most strongly to the top layer bridge site [61]. We therefore considered its dissociation to a conformation where the oxygen and the nitrogen atom are both bound to three platinum atoms, as depicted in Fig. 7. For this situation, we find that the adsorbed NO molecule is more favorable than the corresponding dissociated product by 0.345 eV. The arguments also apply to Pt{1 1 1} [63] and Pt{0 0 1} [58]. Moreover, we find on Pt{0 1 1} (1 × 2) that applying an external electric field disfavors the dissociated product even more. Indeed, if one applies a field of 5 V/nm or 10 V/nm, the energy difference between the two conformations increases to 0.385 eV and 0.475 eV, respectively. In summary, in all of the examined cases, the application of an external electric field disfavors the adsorption of the dissociated product with respect to the molecularly adsorbed form of a single NO molecule.

The situation changes if one considers the formation of a $(NO)_2$ dimer, which would dissociate to form nitrous oxide and an adsorbed oxygen atom:

$$NO(ad) + NO(ad) \rightarrow (NO)_2(ad) \rightarrow N_2O(gas) + O(ad) \quad (9)$$

This reaction mechanism has been found to have a much smaller barrier of 0.32 eV [64] than the alternative mechanism:

$$NO(ad) + N(ad) \rightarrow N_2O(gas) \quad (10)$$

which has been reported to have a barrier exceeding 2.0 eV on a Pt{1 1 2} surface [64]. The pathway via dimer intermediates may be suggested to account for the N_2O (gas) at 296 K as reported in atom probe studies [24] or at 323 K in corresponding field emission studies by Nieuwenhuys and co-workers [65–67]. We also mention that in similar atom probe studies with gold tips both the $(NO)_2$ and N_2O species have been experimentally detected [68]. Here we consider the reaction mechanism as depicted in Fig. 7, which is the same one as originally considered by Liu et al., but now we consider the influence of the external field as well. Although we do find that the formation of the dimer is stable in the absence of an external field, the dissociated products are more favorable energetically by 1.419 eV. The application of an external electric field also allows a stable dimer to adsorb but now, contrary to the other cases examined so far, renders the dissociated products to be even more favorable by increasing the binding energy difference to 1.486 eV at $F = 5$ V/nm and to 1.543 eV at $F = 8$ V/nm.

We finally consider the barriers themselves as shown in Fig. 8. In the absence of a field on a Pt{0 1 1} (1 × 2) surface, the dissociation of NO gives a prohibitively large barrier value exceeding 2.00 eV for the reaction path depicted in Fig. 7. Such a barrier drastically decreases when considering the dissociation of NO on the {2 2 3} plane to 0.89 eV, which is slightly larger than the one found for the corresponding process on the Pt{1 1 2} surface (0.67 eV [62]).

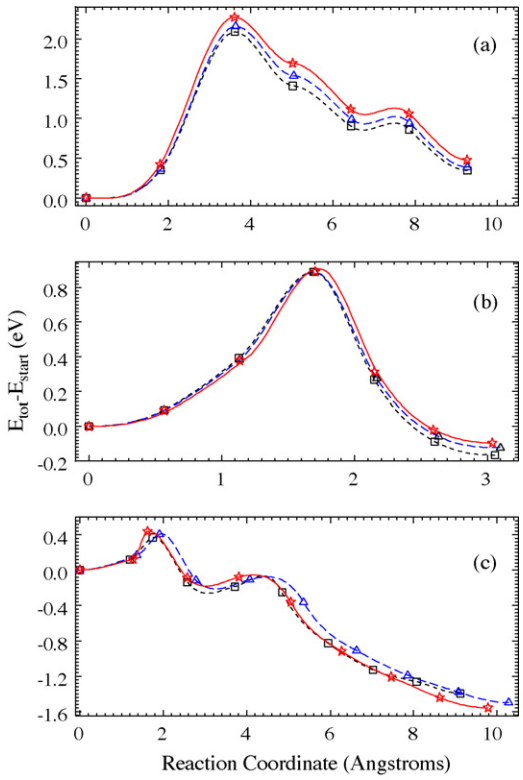

Fig. 8. Dissociation pathways on Pt surfaces using the generalized gradient approximation (GGA) according to Perdew et al. [75]. (a) The dissociation barrier of an NO molecule (increasing reaction coordinate) on a reconstructed Pt{0 1 1} (1 × 2) surface. The surface is modeled with a (2 × 2) cell sampled by a (8 × 8 × 1) **k**-points Monkhost-Pack grid using a five-layer slab with the upper two layer fully relaxed while the other layers where fixed at a theoretical bulk lattice constant of $a = 3.986$ Å. (b) The dissociation of an NO molecule on a Pt{2 2 3} surface with the NO molecule at the base of the step. The Pt{2 2 3} surface was modeled with slabs consisting of six platinum layers in which the uppermost two layers parallel to the step where completely relaxed while the other layers where fixed at the theoretical bulk lattice constant of $a = 3.986$ Å. The surface was modeled by a (2 × 5) cell containing ten surface atoms per layer, sampled by a grid of (8 × 4 × 1) **k**-points. (c) The dissociation of the $(NO)_2$ dimer with the dimer molecule at the base of Pt{223} surface. The same unit cell was used as in (b), but it was sampled with a slightly coarser grid of (4 × 2 × 1) **k**-points with the theoretical bulk lattice constant set to $a = 3.985$ Å. The continuous lines are cubic spline interpolations between the intermediate values at an electric field of 10 V/nm (solid line in panel a), 8 V/nm (solid lines in panels b and c), 5 V/nm (dashed lines) and 0 V/nm (dotted lines). The vacuum thickness was at least ~10 Å in all cases.

When the dissociation of the dimer is considered, an even smaller barrier is obtained of about 0.37 eV, which is in good agreement with the value found for the corresponding process on the {1 1 2} surface (0.32 eV [64]). Thus the formation of the dimer does lead to a smaller dissociation barrier as compared to other processes considered here.

The electric field's influence on these barriers is also depicted in Fig. 8. On the Pt{0 1 1} (1 × 2) surface, the field slightly increases the dissociation barrier. On the Pt{2 2 3} surface, the change in the barrier height is negligible. However, the field's influence on the reaction path is still significant. Indeed, on Pt{2 2 3} the barrier shifts towards the undissociated product. On the other hand, atom probe results show a significant increase in the amount N_2O^+, O^+ and N_2^+ ions as a function of field strength. As previously reported [55], a plausible explanation of these results would be that there exists a process in which a decrease of the activation barrier occurs with increasing field strength. Although the present calculations do not show such a dependence of the activation barrier on the electric field, this effect is possible for other configurations. The most likely candidate of such a mechanism would be through the $(NO)_2$ dimer, since it shows a very small barrier for its decomposition. Moreover, the decomposition of the $(NO)_2$ dimer, unlike the dissociation of NO, shows to be further favored with the application of an external electric field (see Fig. 8c). Here we have concentrated our efforts on the base of the step site. However, other reaction mechanisms involving the $(NO)_2$ dimer have been reported to occur on the step site [64]. In future work, we will examine such alternative mechanisms since it is felt that the key to an understanding of the catalytic reaction of NO by hydrogen on Pt is in the proper description of the NO adsorption and reaction behavior. This will finally lead to a reasonable mechanistic network able to explain the kinetic instabilities in the reduction process.

6. Conclusions

This paper has demonstrated that the combination of experiment (using FEM, FIM and atom probe techniques) and theoretical modeling (using DFT and kinetic mean field models) leads into new insights in the study of model catalyst under reaction conditions. Through two case studies we have demonstrated how an external electric field interacts with the various nanofacets that are simultaneously exposed at the tip's surface. Such nanofacets consequently have different catalytic properties which provide the origin of the oscillating nanopatterns as observed in FIM.

On a rhodium field emitter tip, such a structure dependence was shown to be crucial if one wants to explain the chemical clock behavior of the O_2–H_2 reaction in the presence of an electric field, since in its absence there is no subsurface oxygen and thus no oscillations present. The important role of the external electric field is to facilitate the formation of a surface oxide at low oxygen pressures. Indeed, the electric field increases the pressure over the apex of the tip in FIM, because of the interaction of this field with polarizable molecules like O_2 and H_2 [22,23]. On the other hand, and more importantly, it decreases the activation barrier for oxidation of the surface, as we demonstrated in this work. Thus, the electric field, in the present study, turns out to help bridge the gap between low-pressure single-crystal surface studies and high-pressure heterogeneous catalysis.

On a platinum field emitter tip, we examined how an externally applied electric field changes the potential energy landscape for an adsorbed NO molecule. Emphasis was laid on inspecting which pathways are energetically most favorable to account for nitrous oxide formation. A reaction pathway via a $(NO)_2$ species was investigated. Indeed, since the $(NO)_2$ dimer is not strongly bound to the surface, a high NO coverage would be needed for its formation. Such a high NO coverage can be achieved by the application of an electric field since this increases the corresponding NO pressure above the surface [69,70]. This picture would also correlate well with the "vacancy mechanism" first suggested by Ben Nieuwenhuys in which the availability of empty sites is supposed to play a central role in the selectivity of towards N_2O and N_2, with the formation of N_2O being favored when it is low [72–74]. Such an understanding of underlying possesses occurring on the surface is crucial if one wants to develop a comprehensive model of the oscillations as observed in FEM or FIM. Indeed, even in a seemingly simpler system, such as when Pt{0 0 1} is exposed to NO and H_2 [51–53], many more reaction pathways may result as compared to the O_2–H_2 reaction on a Rh field emitter tip. It is therefore essential to determine which reaction pathways one must take into account in a corresponding kinetic model of such regularly oscillating systems, as is the case of the NO_2 reduction with hydrogen on a Pt tip [71], in order to embrace the complexity of these systems.

Acknowledgements

TV and JSM (postdoctoral researchers) gratefully thank the Fonds de la Recherche Scientifique (F.R.S.-FNRS) for financial support. JSM would also like to thank Yannick De Decker for useful discussions on the Pt project. This research is financially supported by the "Communauté française de Belgique" (contract "Actions de Recherche Concertées" no. 04/09-312).

References

[1] R. Imbihl, Prog. Surf. Sci. 44 (1993) 185.
[2] M. Slinko, N. Jaeger, Oscillating heterogeneous catalytic systems, Studies in Surface Science and Catalysis, vol. 86, Elsevier, Amsterdam, 1994.
[3] R. Imbihl, G. Ertl, Chem. Rev. 95 (1995) 697.
[4] R. Imbihl, Catal. Today 105 (2005) 206.
[5] V. Gorodetskii, J. Lauterbach, H.-H. Rotermund, J.H. Block, G. Ertl, Nature 370 (1994) 276.
[6] M.F.H. van Tol, M. Gilbert, B.E. Nieuwenhuys, Catal. Lett. 16 (1992) 297.
[7] P. Cobden, C. de Wolf, M. Smirnov, A. Makeev, B. Nieuwenhuys, J. Mol. Catal. A158 (2000) 115.
[8] C. de Wolf, B. Nieuwenhuys, Catal. Today 70 (2001) 287.
[9] P.L. Dulong, L.G. Thénard, Ann. Chim. Phys. 23 (1823) 440.
[10] P.L. Dulong, L.G. Thénard, Ann. Chim. Phys. 24 (1823) 380.
[11] M. Faraday, Philos. Trans. R. Soc. 124 (1834) 55.
[12] S. Völkening, K. Bedüftig, K. Jacobi, J. Wintterlin, G. Ertl, Phys. Rev. Lett. 83 (1999) 2672.
[13] J. Gustafson, A. Mikkelsen, M. Borg, E.L.L. Köhler, G. Kresse, M. Schmid, P. Varga, J. Yuhara, X. Torrelles, C. Quirós, J.N. Andersen, Phys. Rev. Lett. 92 (2004) 126102.
[14] J. Gustafson, A. Mikkelsen, M. Borg, J.N. Andersen, E. Lundgren, C. Klein, W. Hofer, M. Schmid, P. Varga, L. Köhler, G. Kresse, N. Kasper, A. Stierle, H. Dosch, Phys. Rev. B 71 (2005) 115442.
[15] C. Dri, C. Africh, F. Esch, G. Comelli, O. Dubay, L. Köhler, F. Mittendorfer, G. Kresse, J. Chem. Phys. 125 (2006) 094701.
[16] J. Gustafson, A. Resta, A. Mikkelsen, R. Westerström, J.N. Anderson, E. Lundgren, J. Weissenrieder, M. Schmid, P. Varga, N. Kaspaer, X. Torrelles, S. Ferrer, F. Mittendorfer, G. Kresse, Phys. Rev. B 74 (2006) 035401.
[17] J. Klikovits, M. Schmid, L.R. Merte, P. Varga, R. Westerström, A. Resta, J.N. Andersen, J. Gustafson, A. Mikkelsen, E. Lundgren, F. Mittendorfer, G. Kresse, Phys. Rev. Lett. 101 (2008) 266104.
[18] P. Nolte, A. Stierle, N.Y. Jin-Phillip, N. Krasper, T.U. Schulli, H. Dosch, Science. 321 (2008) 1654.
[19] P. Dudin, A. Barinov, L. Gregoratti, M. Kiskinova, F. Esch, C. Dri, C. Africh, C. Comelli, J. Phys. Chem. B109 (2005) 13649.
[20] J. Klikovits, M. Schmid, J. Gustafson, A. Mikklsen, A. Resta, E. Lundgren, J.N. Andersen, P. Varga, J. Phys. Chem. B110 (2006) 9966.
[21] N. Ernst, G. Bozdech, V. Gorodetskii, H.J. Kreuzer, R.C.L. Wang, J. Block, Surf. Sci. 318 (1994) L1221.
[22] J.-S. McEwen, P. Gaspard, T. Visart de Bocarmé, N. Kruse, P. Natl. Acad. Sci. U.S.A. 106 (2009) 3006.
[23] J.-S. McEwen, P. Gaspard, T. Visart de Bocarmé, N. Kruse, J. Phys. Chem. C113 (2009) 17045.
[24] N. Kruse, J.H. Block, in: A. Crucq, A. Frennet (editors), Proceedings of the 1st International Congress on Catalysis and Automotive Pollution Control, Elsevier, Amsterdam, 1987, vol. 30 of Stud. Surf. Sci. Catal., p. 173.
[25] M. Kiskinova, G. Pirug, H.P. Bonzel, Surf. Sci. 140 (1984) 1.
[26] A. Gaussmann, N. Kruse, Catal. Lett. 1 (1991) 305.
[27] M.L. Wagner, L.D. Schmidt, J. Chem. Phys. 99 (1995) 805.
[28] B.A. Gurney, W. Ho, J. Chem. Phys. 87 (1987) 5562.
[29] F.C.V. der Lage, H.A. Bethe, Phys. Rev. 71 (1947) 612.
[30] G. Kresse, J. Furthmüller, Phys. Rev. B54 (1996) 11169.
[31] G. Kresse, J. Furthmüller, Computat. Mat. Sci. 6 (1996) 15.
[32] http://cms.mpi.univie.ac.at/vasp/.
[33] J.-S. McEwen, P. Gaspard, F. Mittendorfer, T. Visart de Bocarmé, N. Kruse, Chem. Phys. Lett. 452 (2008) 133.
[34] Y. De Decker, F. Baras, N. Kruse, G. Nicolis, J. Chem. Phys. 117 (2002) 10244.
[35] H. Jóhnsson, G. Mills, K.W. Jacobsen, Classical and Quantum Dynamics in Condensed Phase Simulations, World Scientific, Singapore, 1998.
[36] A. Makeev, N. Janssen, P. Cobden, M. Slinko, B. Nieuwenhuys, J. Chem. Phys. 107 (1997) 965.
[37] N. Janssen, A. Schaak, B. Nieuwenhuys, R. Imbihl, Surf. Sci. 364 (1996) L555.
[38] G. Nicolis, Introduction to Nonlinear Science, Cambridge University Press, 1995.
[39] T. Visart de Bocarmé, T. Bär, N. Kruse, Ultramicroscopy 89 (2001) 75.
[40] T. Visart de Bocarmé, G. Beketov, N. Kruse, Surf. Interface Anal. 36 (2004) 522.
[41] J. Boissonade, P. de Kepper, J. Phys. Chem. 84 (1980) 501.
[42] E. Lundgren, G. Gustafson, A. Resta, J. Weissenrieder, A. Mikkelsen, J.N. Andersen, L. Köhler, G. Kresse, J. Klikovits, A. Biederman, M. Schmid, P. Varga, J. Electron. Spectrosc. Relat. Phenom. 144–147 (2005) 367.
[43] R. Westerström, J.G. Wang, M.D. Ackermann, J. Gustafson, A. Resta, A. Mikkelsen, J.N. Andersen, E. Lundgren, O. Balmes, X. Torrelles, J.W.M. Frenken, B. Hammer, J. Phys.: Condens. Matter 20 (2008) 184018.
[44] J. Gustafson, R. Westerström, A. Mikkelsen, X. Torrelles, O. Balmes, N. Bovet, J.N. Andersen, C.J. Baddeley, E. Lundgren, Phys. Rev. B78 (2008) 045423.
[45] J.I. Flege, P. Sutter, Phys. Rev. B78 (2008) 153402.
[46] J. Gustafson, R. Westerström, A. Resta, A. Mikkelsen, J. Andersen, O. Balmes, X. Torrelles, M. Schmid, P. Varga, B. Hammer, G. Kresse, C.J. Baddeley, E. Lundgren, Catal. Today 145 (2009) 227.
[47] M. Willinger, R. Schlögl, T. Visart de Bocarmé, N. Kruse, in preparation.
[48] L.J. Richter, W. Ho, J. Vac. Sci. Technol. A5 (1987) 453.
[49] P.A.J. Bagot, T. Visart de Bocarmé, A. Cerezo, G.D.W. Smith, Surf. Sci. 600 (2006) 3028.
[50] C. Voss, N. Kruse, Appl. Surf. Sci. 87–88 (1995) 127.
[51] A.G. Makeev, B.E. Nieuwenhuys, J. Chem. Phys. 108 (1998) 3740.
[52] M. Slinko, T. Fink, T. Löher, H.H. Madden, S.J. Lombardo, R. Imbihl, G. Ertl, Surf. Sci. 264 (1992) 157.
[53] S.J. Lombardo, T. Fink, R. Imbihl, J. Chem. Phys. 98 (1993) 5526.
[54] Y. De Decker, Private Communication.
[55] H.J. Kreuzer, L.C. Wang, J. Chem. Phys. 93 (1990) 6065.
[56] Z.-P. Liu, S.J. Jenkins, D.A. King, J. Am. Chem. Soc. 125 (2003) 14660.
[57] J.-S. McEwen, A. Eichler, J. Chem. Phys. 126 (2007) 094701.
[58] A. Eichler, J. Hafner, Chem. Phys. Lett. 343 (2001) 383.
[59] A. Eichler, J. Hafner, J. Catal. 204 (2001) 118.
[60] E.H.G. Backus, A. Eichler, M.L. Grecea, A.W. Kleyn, M. Bonn, J. Chem. Phys. 121 (2004) 7946.
[61] Q. Ge, W.A. Brown, R.K. Sharma, D.A. King, J. Chem. Phys. 110 (1999) 12082.
[62] Q. Ge, M. Neurock, J. Am. Chem. Soc. 126 (2004) 1551.
[63] M. Gajdoš, J. Hafner, A. Eichler, J. Phys.: Condens. Matter. 18 (2006) 41.
[64] R. Burch, S.T. Daniells, P. Hu, J. Chem. Phys. 121 (2004) 2737.
[65] H. Hirano, T. Yamada, K.I. Tanaka, J. Siera, P. Cobden, B.E. Nieuwenhuys, Surf. Sci. 262 (1992) 97.
[66] H. Hirano, T. Yamada, K.I. Tanaka, J. Siera, B.E. Nieuwenhuys, Stud. Surf. Sci. Catal. 75 (1993) 345.
[67] Y.J. Mergler, B.E. Nieuwenhuys, Appl. Catal. B12 (1997) 95.
[68] T.D. Chau, T. Visart de Bocarmé, N. Kruse, Catal. Lett. 98 (2004) 85.
[69] E.A. Guggenheim, Encyclopedia of Physics, vol. III/2, Springer-Verlag, Berlin, 1959, pp. 1–118.
[70] N.D. Bridge, A.D. Buckingham, Proc. R. Soc. Lon. Ser. A295 (1966) 334.
[71] C. Voss, N. Kruse, Appl. Surf. Sci. 94–95 (1996) 186.
[72] J. Siera, P. Cobden, K. Tanaka, B.E. Nieuwenhuys, Catal. Lett. 10 (1991) 335.
[73] P.D. Cobden, J. Siera, B.E. Nieuwenhuys, J. Vac. Sci. Technol. A10 (1992) 2487.
[74] N.M.H. Janssen, P.D. Cobden, B.E. Nieuwenhuys, J. Phys.: Condens. Matter 9 (1997) 1889.
[75] J.P. Perdew, J.A. Chevary, S.H. Vosko, K.A. Jackson, M.R. Pederson, D.J. Singh, C. Fiolhais, Phys. Rev. B46 (1992) 6671.